A Robust CFL Condition for the Discontinuous Galerkin Method on Triangular Meshes

N. Chalmers* and L. Krivodonova†

Abstract

When the discontinuous Galerkin (DG) method is applied to hyperbolic problems in two dimensions on triangular meshes and paired with an explicit time integration scheme, an exact CFL condition is not known. The stability condition which is most usually implemented involves scaling the time step by the smallest radius of the inscribed circle in every cell. However, this is known to not provide a tight bound on the largest possible stable time step in some cases. In this paper, we apply the DG method to a simple linear problem and derive a PDE which is satisfied by the numerical solution itself. By applying classical Fourier analysis to the solutions of this PDE we find a natural scaling of the spectrum of the DG spatial operator by a parameter h_j, which can be seen to be the width of the cell Ω_j along the characteristic direction of flow. We use this parameter to propose a new CFL condition and show through several numerical examples that we are able to select significantly larger time steps than usually obtained using the inscribed radii of the computational cells.

1 Introduction

When the discontinuous Galerkin method with the p-th degree basis is applied to hyperbolic problems in one dimension with a standard pairing with an order $(p+1)$ explicit Runge-Kutta (RK) method, it is known [5] that an effective CFL condition is

$$\Delta t \leqslant \frac{1}{2p+1} \min_j \frac{h_j}{|a_j|} \tag{1}$$

where h_j is the size of mesh cell j and $|a_j|$ is the largest in magnitude wave speed in that cell. Other choices of time integrators will naturally lead to different CFL numbers. A table of CFL numbers for explicit Runge-Kutta time integrators and DG methods of various orders can be found in [5].

The order-dependent CFL number $\frac{1}{2p+1}$ is caused by the growth of the spectrum of the spatial discretization operator of the semi-discrete scheme at the rate slightly slower than $\mathcal{O}(p^2)$ [10] whereas the size of the absolute stability regions of explicit Runge-Kutta methods grow linearly with p [8]. While CFL condition (1) has been proven for $p = 0$ and $p = 1$ in [4], the remaining CFL numbers were verified numerically. The reason being that both the spectrum of the DG spatial

*Email: bnachalm@uwaterloo.ca

†Email: lgk@uwaterloo.ca. Corresponding author.

operator and the absolute stability regions of the RK methods are defined through implicit functions. Several approaches to improving the CFL number in one dimension have been proposed, such as using additional stages in explicit RK time integration [12, 16], using specially selected explicit RK methods [13, 14], altering the spectrum of the DG spatial operator through flux modifications [2], and filtering the numerical solution using covolume meshes [17].

On triangular grids in two dimensions, an appropriate CFL condition for the DG scheme is more difficult to obtain. Originally, the stability condition

$$\Delta t \leqslant \frac{1}{2p+1} \min_j \frac{r_j}{||\mathbf{a}_j||}, \tag{2}$$

was proposed and supported with numerical evidence [3], where r_j is the radius of the inscribed circle in cell j and $||\mathbf{a}_j||$ is the magnitude of the largest wave speed in that cell. While this CFL condition provides a stable time step, it is known to not be a tight bound and in some cases a much larger time step can be taken. The main difficulty in finding optimal CFL numbers is that the spectrum of the DG discretization depends on the orientation of the triangular cells with respect to the flow direction [9] and the shape of these triangles. In [11], eigenvalues of the DG spatial operator were numerically computed for two uniform triangular mesh configurations and for various flow directions. The exact CFL numbers were then computed for a number of strong stability preserving (SSP) Runge-Kutta methods. The authors proposed a CFL condition that uses the radius of the largest circle that is entirely contained within all elements sharing a vertex. While the authors demonstrated the efficacy of this CFL condition, their numerical testing considered only these two grid configurations. A similar analysis was preformed in [15] where this approach was extended to a variety of triangle shapes. The authors considered five different measures of cell size and concluded that none were completely effective for all flow directions and cell shapes but the minimum cell height and the inscribed circle radius appeared to be the most appropriate measures. In both [11] and [15], the CFL estimates did not incorporate flow direction. Instead, the minimum CFL number was chosen over all flow directions.

In this paper, we propose a CFL condition that is based on a new measure of cell size h_j, which depends on the characteristic flow direction in cell Ω_j. Geometrically, h_j is the width of Ω_j along the direction of flow. By considering a linear advection problem on a square which has been subdivided into triangular cells we perform classical von Neumann analysis in order to derive a simple linear system which we can use to calculate the spectrum of the entire DG spatial operator. We then show that the scaling of the spectrum by the parameter h_j arises naturally, and that the spectrum also depends on a parameter $\theta \in [0, 1]$ which can be viewed as giving a measure of the relative flow direction in each cell. Our numerical experiments reveal that the overall size of the spectrum is not very sensitive to the parameter θ. Specifically, the size of the spectrum of the DG spatial operator scales by at most 5.5% as θ varies. This implies that the majority of the scaling of the spectrum is captured by the measure h_j. Consequently, we propose a new CFL condition

$$\Delta t \leqslant CFL \ \min_j \frac{h_j}{||\mathbf{a}||}. \tag{3}$$

When pairing the DG spatial discretization with an explicit Runge-Kutta-$(p+1)$ time integration, we show that

$$CFL = \frac{1}{(2p+1)\left(1 + \frac{4}{(p+2)^2}\right)}$$

provides a fairly tight bound on the time step Δt up to at least degree $p = 10$. Specifically, this CFL number is within 5% of the exact CFL numbers we compute.

We then generalize the conclusions from this scalar linear problem to non-linear systems of conservation laws. In the case of nonlinear scalar equations, this stability analysis extends naturally through a standard linearization argument. In the case of systems, however, there may be characteristic fields that do not have a distinct flow direction but rather propagate in infinite directions forming a characteristic Monge cone. In this case, a minimazation can be performed over all directions which may be computationally expensive. Otherwise, the minimum cell height and the maximum wave speed for the characteristic field may simply be chosen.

The outline of the paper is as follows. We first introduce the DG scheme for a linear advection problem in two dimensions and investigate the spectrum of the method by considering a uniform mesh of triangles. We then apply classical von Neumann analysis to derive a simple linear system which can be used to easily compute the entire spectrum of the DG spatial operator. We then compute the exact CFL numbers of the DG schemes when using our proposed CFL condition (3) and various explicit RK time discretizations. We also show that the two-dimensional spectra can be scaled within the spectra of one-dimensional DG schemes of the same order. We conclude by providing several numerical examples which demonstrate the efficacy of the CFL condition (3) on unstructured grids for both linear and non-linear problems.

2 The DG Discretization

To introduce the notation, we briefly describe the DG scheme applied to a simple linear advection problem in two dimensions on a computational mesh of triangles. We consider the linear advection equation

$$u_t + \mathbf{a} \cdot \nabla u = 0, \tag{4}$$

where $\mathbf{a} = (a, b)^T$, on a two dimensional domain $\Omega \subset \mathbb{R}^2$ subject to the initial condition $u(x, y, 0) = u_0(x, y)$ and suitable boundary conditions. We begin as usual by discretizing the domain Ω into non-overlapping triangular cells Ω_j, $j = 1, 2, ..., N$, so that

$$\Omega = \bigcup_{j=1}^{N} \Omega_j.$$

To obtain a more convenient expression for computations, we map each cell Ω_j to a computational cell Ω_0. We denote the vertices of Ω_j by (x_1, y_1), (x_2, y_2), and (x_3, y_3), traveling counter-clockwise and map Ω_j to the cell Ω_0 in the variables (ξ, η), which has vertices located at (0,0), (1,0), and (0,1) (see Figure 1). This mapping is given by

$$\begin{pmatrix} x \\ y \\ 1 \end{pmatrix} = \begin{pmatrix} x_1 & x_2 & x_3 \\ y_1 & y_2 & y_3 \\ 1 & 1 & 1 \end{pmatrix} \begin{pmatrix} 1 - \xi - \eta \\ \xi \\ \eta \end{pmatrix}, \tag{5}$$

The Jacobian matrix for this transformation is constant and given by

$$J_j = \begin{pmatrix} x_\xi & x_\eta \\ y_\xi & y_\eta \end{pmatrix} = \begin{pmatrix} x_2 - x_1 & x_3 - x_1 \\ y_2 - y_1 & y_3 - y_1 \end{pmatrix}, \tag{6}$$

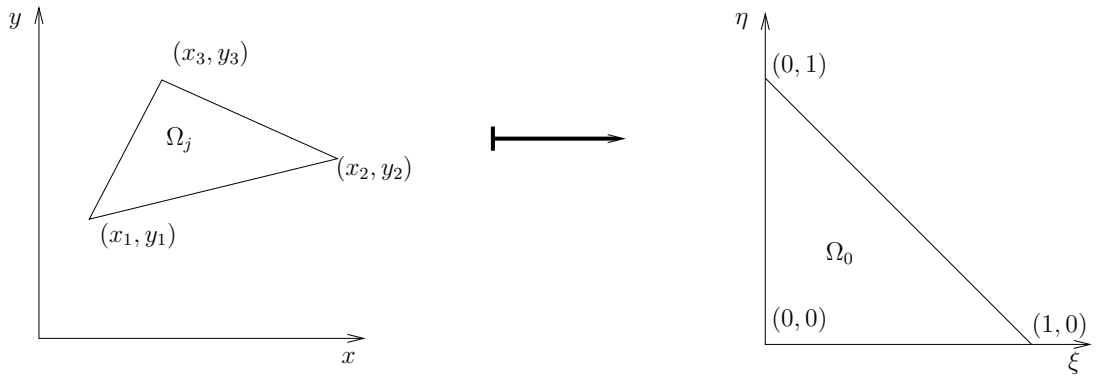

Figure 1: The transformation (5) maps each computational cell Ω_j to the canonical cell Ω_0.

and satisfies $\det(J_j) = 2|\Omega_j|$, where $|\Omega_j|$ is the size of element Ω_j. Upon mapping the linear problem (4) to the canonical triangle Ω_0 we obtain the scaled problem

$$u_t + \boldsymbol{\alpha}_j \cdot \nabla u = 0, \tag{7}$$

where the ∇ operator is now understood as a gradient in (ξ, η)-space and

$$\boldsymbol{\alpha}_j = (\alpha_j, \beta_j) = \mathbf{a} \cdot (J_j^{-1})^T \tag{8}$$

is a scaled flow direction.

We multiply the equation (7) by a test function v, integrate over the cell Ω_0, and apply the divergence theorem to obtain the weak form of the conservation law

$$\frac{d}{dt} \iint_{\Omega_0} u\, v \; dA - \iint_{\Omega_0} u\, \boldsymbol{\alpha}_j \cdot \nabla v \; dA + \oint_{\partial\Omega_0} \mathbf{n} \cdot \boldsymbol{\alpha}_j \, u\, v \; ds = 0, \tag{9}$$

where $\partial\Omega_0$ is the boundary of Ω_0, oriented counter-clockwise, and $\mathbf{n}$ is the outward-facing normal vector to $\partial\Omega_0$. In each cell, we approximate the exact solution u by a polynomial $U_j \in \mathbf{P}_p$ where

$$\mathbf{P}_p = \text{span}\{\xi^{k-i}\eta^i | k = 0, \ldots p, i = 0, \ldots k\}$$

is space of polynomials of degree up to p. We also obtain a Galerkin formulation by taking the test functions v to be from the same space, $\mathbf{P}_p$. Using this approximation in (9) we obtain the semi-discrete DG formulation

$$\frac{d}{dt} \iint_{\Omega_0} U_j V \; dA - \iint_{\Omega_0} U_j\, \boldsymbol{\alpha}_j \cdot \nabla V \; dA + \oint_{\partial\Omega_0} \mathbf{n} \cdot \boldsymbol{\alpha}_j \, \mathbf{U}_j^* V \; ds = 0, \tag{10}$$

for all $V \in \mathbf{P}_p$. Note that since the numerical solution is potentially multi-valued along $\partial\Omega_j$ we replace the exact solution u by a Riemann state U_j^* along the boundary $\partial\Omega_0$ which is determined using the values of the numerical solution on both sides of the boundary. For this linear problem we will determine U_j^* using an upwind flux. That is, if we denote the value of the numerical solution in a neighboring cell on the other side of $\partial\Omega_0$ by $\mathbf{U}_{j+}$ then we choose U_j^* as

$$U_j^* = \begin{cases} U_j, & \boldsymbol{\alpha}_j \cdot \mathbf{n} \geqslant 0, \\ U_{j+}, & \boldsymbol{\alpha}_j \cdot \mathbf{n} < 0. \end{cases} \tag{11}$$

To proceed, we choose the Dubiner basis [6] for the polynomial space $\mathbf{P}_p$. These basis functions are given by

$$\psi_{ki}(\xi,\eta) = \sqrt{(2i+1)(2k+2)}P_{k-i}^{0,2i+1}(1-2\xi)\cdot(1-\xi)^i P_i\left(1-\frac{2\eta}{1-\xi}\right),$$

for $k = 0,\ldots,p$ and $i = 0,\ldots,k$, where $P_{k-i}^{0,2i+1}$ is the degree $k-i$ Jacobi polynomial with parameters 0 and $2i+1$ and P_i is the degree i Legendre polynomial. These basis polynomials are orthonormal on the computational cell Ω_0, i.e.,

$$\iint_{\Omega_0} \psi_{ki}\psi_{lm}\, dA = \delta_{kl}\delta_{im}, \tag{12}$$

where δ_{kl} is the Kronecker delta function. We write the numerical solution as a linear combination of these basis polynomials, i.e.,

$$U_j = \sum_{m=0}^{p}\sum_{l=0}^{m} c_{jml}\psi_{ml}(\xi,\eta), \tag{13}$$

and use this in (10) taking $V = \psi_{ki}$ for $k = 0,\ldots,p$ and $i = 0,\ldots,k$ and using the orthogonality (12) to obtain $\frac{1}{2}(p+1)(p+2)$ equations

$$\frac{d}{dt}c_{jki} = \iint_{\Omega_0} U_j\,\boldsymbol{\alpha}_j\cdot\nabla\psi_{ki}\, dA - \oint_{\partial\Omega_0}\mathbf{n}\cdot\boldsymbol{\alpha}_j\, U_j^*\psi_{ki}\, ds. \tag{14}$$

The spatial discretization is then completed by approximating the volume integral using a quadrature rule over Ω_0 [7] and approximating the integral along each edge of $\partial\Omega_0$ by using an appropriate one-dimensional quadrature. We then obtain a fully-discrete scheme by time evolving the solution coefficients using some appropriate time-stepping scheme.

3 Spectrum of Spatial Discretization

We note that the right hand side of (14) is a linear function of the solution coefficients c_{jki}. Thus, the semi-discrete DG scheme can be written in vector form as

$$\frac{d}{dt}\mathbf{c} = L\mathbf{c}, \tag{15}$$

where $\mathbf{c} = [c_{100}, c_{110}, \ldots, c_{1pp}, c_{200}, \ldots, c_{Npp}]^T$ and L is a $\frac{1}{2}(p+1)(p+2)N \times \frac{1}{2}(p+1)(p+2)N$ matrix. The stability restriction of the time-stepping will then depend on the size of the spectrum of L. The difficulty which becomes apparent from (14) is that the matrix L, and hence its spectrum, depends on the scaled flow direction $\boldsymbol{\alpha}_j$ in each cell, which itself depends on both the direction of flow $\mathbf{a}$ and the orientation of the cell. It is therefore unclear how the spectrum of L will scale under mesh refinement.

To begin, we assume without loss of generality that the verticies of Ω_j have been ordered in such a way that after the transformation (5) to the canonical cell we have that α_j and β_j have the same sign, or one of the is equal to zero. We then proceed by applying another change of variables to (14), given by

$$\begin{pmatrix}\zeta\\ \sigma\end{pmatrix} = \begin{pmatrix}1 & 1\\ \theta_j - 1 & \theta_j\end{pmatrix}\begin{pmatrix}\xi\\ \eta\end{pmatrix}. \tag{16}$$

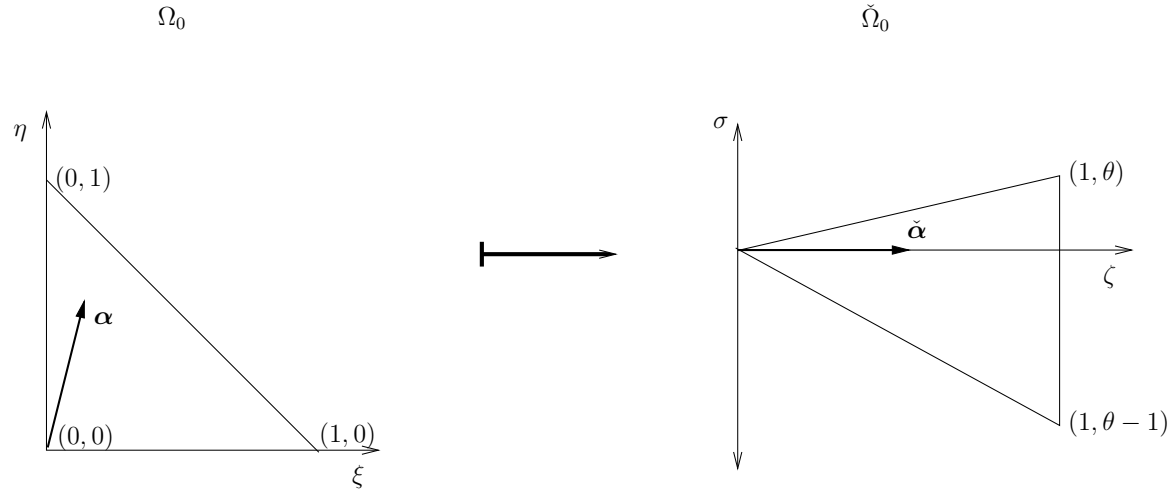

Figure 2: The transformation (16) maps the coordinate system so that the direction of flow is along the ζ-axis.

Here $\theta_j = \frac{\alpha_j}{\alpha_j+\beta_j}$ is a parameter in $[0,1]$ which can be viewed as giving a measure of the flow direction $\boldsymbol{\alpha}_j$ since $\theta_j = 0$ occurs when $\alpha_j = 0$ and $\theta_j = 1$ occurs when $\beta_j = 0$. We will use the check accent to denote objects in these new coordinates. Hence, the image of Ω_0 under (16) is denoted by $\check{\Omega}_0$. We observe that $\check{\Omega}_0$ has vertices at $(0,0)$, $(1,\theta_j - 1)$, and $(1,\theta_j)$. Note also that the transformation (16) preserves the area of Ω_0. The flow direction $\check{\boldsymbol{\alpha}}_j$ in the (ζ,σ)-coordinates is given by

$$\begin{aligned}\check{\boldsymbol{\alpha}}_j &= \boldsymbol{\alpha}_j \begin{pmatrix} 1 & \theta_j - 1 \\ 1 & \theta_j \end{pmatrix} \\ &= (\alpha_j + \beta_j, 0).\end{aligned}$$

Hence, $\check{\Omega}_0$ is such that the flow direction $\check{\boldsymbol{\alpha}}_j$ is along the ζ-axis (see Figure 2). Consequently, upon transforming the ∇ operator to the (ζ,σ) coordinates we find that the operator $\boldsymbol{\alpha}_j \cdot \nabla$ becomes $(\alpha_j + \beta_j)\frac{\partial}{\partial \zeta}$ in the new coordinate system.

We also introduce a new small parameter $h_j = \frac{||\mathbf{a}||}{\alpha_j+\beta_j}$ which will tend to zero under mesh refinement. In fact, h_j is the width of the cell Ω_j along the direction of flow $\mathbf{a}$. To see this, first note that from the definition of the scaled velocity $\boldsymbol{\alpha}_j$ in (8) we can write

$$\alpha_j = \frac{a(y_3 - y_1) - b(x_3 - x_1)}{(x_2 - x_1)(y_3 - y_1) - (x_3 - x_1)(y_2 - y_1)},$$

$$\beta_j = \frac{-a(y_2 - y_1) + b(x_2 - x_1)}{(x_2 - x_1)(y_3 - y_1) - (x_3 - x_1)(y_2 - y_1)}.$$

Hence, we can write

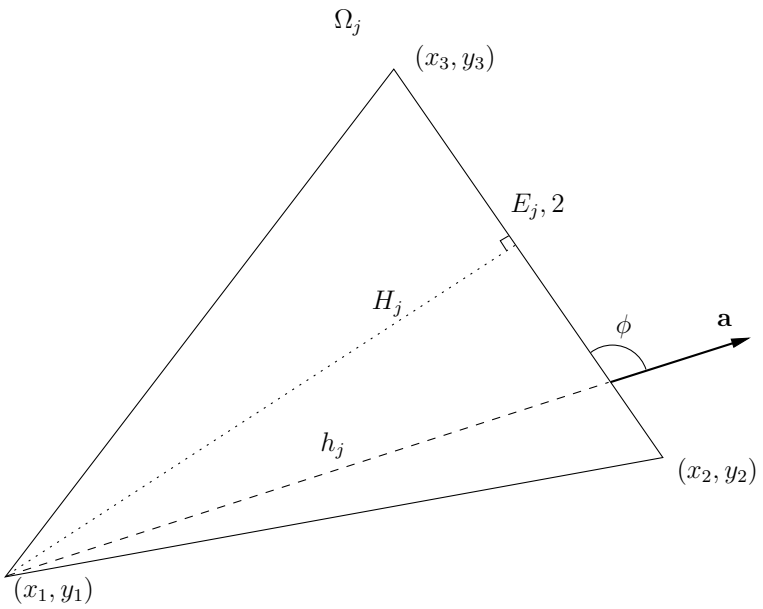

Figure 3: Diagram of the cell Ω_j showing the parameter h_j. We see that h_j is the width of Ω_j along the direction of flow $\mathbf{a}$.

$$\begin{aligned} h_j &= \frac{||\mathbf{a}||}{\alpha_j + \beta_j} \\ &= ||\mathbf{a}|| \frac{(x_2 - x_1)(y_3 - y_1) - (x_3 - x_1)(y_2 - y_1)}{a(y_3 - y_2) - b(x_3 - x_2)} \\ &= ||\mathbf{a}|| \frac{\det J_j}{\mathbf{a} \cdot (y_3 - y_2, -(x_3 - x_2))} \\ &= \frac{2|\Omega_j|}{|E_{j,2}| \sin \phi}. \end{aligned} \tag{17}$$

Here we have used the notation that ϕ is the angle between $\mathbf{a}$ and $E_{j,2}$, where $E_{j,2}$ is the side of Ω_j which connects (x_2, y_2) and (x_3, y_3) (see Figure 3). We have also used that $\det J_j = 2|\Omega_j|$. If we write the area of cell Ω_j as $|\Omega_j| = \frac{1}{2}|E_{j,2}|H_j$, where H_j is the height of cell Ω_j measured from the vertex (x_1, y_1) to the edge $E_{j,2}$, then we see that (17) implies that $h_j \sin \phi = H_j$. From the definition of ϕ we see that h_j is the width of cell Ω_j along the direction of flow $\mathbf{a}$.

Transforming (14) to this new coordinate system using (16) we obtain the following semi-discrete DG formulation

$$\frac{d}{dt} c_{jki} = \frac{||\mathbf{a}||}{h_j} \left(\iint_{\check{\Omega}_0} \check{U}_j \frac{\partial}{\partial \zeta} \check{\psi}_{ki} \, dA - \oint_{\partial \check{\Omega}_0} n_\zeta \check{U}_j^* \check{\psi}_{ki} \, ds \right). \tag{18}$$

Here we have used the notation that n_ζ is the first coordinate of the normal vector $\check{\mathbf{n}} = (n_\zeta, n_\sigma)^T$ in the (ζ, σ)-coordinates, and $\check{\psi}_{ki}$ are the polynomial basis functions now evaluated in the (ζ, σ)-coordinates. The numerical solution $\check{U}_j$ is now understood to be evaluated in (ζ, σ)-coordinates as well.

Note now that the expression within the parentheses on the right hand side of (18) is a linear function of the solution coefficients c_{jki} and depends only on the parameter θ, which remains

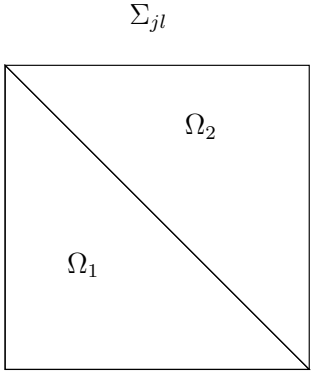

Figure 4: Diagram of a square cell Σ_{jl} and the two triangular sub cells Ω_1 Ω_2.

bounded between 0 and 1 under mesh refinement. Therefore, we find that the DG spatial discretization on the right hand side of (18) will be scaled purely by the small parameter $\frac{1}{h_j}$. This implies that the spectrum of the spatial operator is effectively scaled by this factor as well, provided that the spectrum does not vary significantly with θ. We are therefore motivated to investigate what effects the parameter θ has on the spectrum of the DG spatial discretization and whether h_j is an effective scaling factor in the CFL condition of the scheme. To do this, we proceed by making the simplifying assumption of a uniform mesh in order to obtain a simple way to compute the entire spectrum of the spatial operator.

4 Analysis of Spectrum

In this section we consider a simple uniform mesh in order to derive a simple way to compute the spectral values of the DG spatial discretization operator. Specifically, we consider the linear problem (4) on the unit square domain $\Sigma = [0,1] \times [0,1]$ with periodic boundary conditions. We consider a particularly simple uniform computational mesh found by partitioning Σ into $N \times M$ rectangles $\Sigma_{nm} = [x_n, x_{n+1}] \times [y_m, y_{m+1}]$ of size $\Delta x \times \Delta y$, then dividing each square into two triangles along lines connecting the points (x_{n+1}, y_m) and (x_n, y_{m+1}). We label the two triangular cells inside Σ_{nm} as $\Omega_{nm,1}$ and $\Omega_{nm,2}$. We begin by mapping the triangular cells $\Omega_{nm,1}$ and $\Omega_{nm,2}$ to the canonical triangle Ω_0 using the mappings

$$\begin{pmatrix} x \\ y \end{pmatrix} = \begin{pmatrix} \Delta x \xi + x_n \\ \Delta y \eta + y_m \end{pmatrix}, \tag{19}$$

and

$$\begin{pmatrix} x \\ y \end{pmatrix} = \begin{pmatrix} -\Delta x \xi + x_{n+1} \\ -\Delta y \eta + y_{m+1} \end{pmatrix} \tag{20}$$

respectively. On each cell, the flow direction is given by $\boldsymbol{\alpha} = \left[\frac{a}{\Delta x}, \frac{b}{\Delta y}\right]$. Next, as is usual in von Neumann stability analysis, we assume the numerical solution on the triangular cell $\Omega_{nm,l}$, denoted ny $U_{nm,l}$, has the form

$$U_{nm,l}(\xi, \eta, t) = \widehat{U}_l(\xi, \eta, t) \exp\left(n \Delta x \kappa_x + m \Delta y \kappa_y\right), \tag{21}$$

where $\exp(\Delta x\kappa_x)$ is an N-th root of unity, $\exp(\Delta y\kappa_y)$ is an M-th root of unity, and $\widehat{U}_l(\xi,\eta,t)$ is a degree p polynomial in ξ and η. We denote the solution coefficients of $\widehat{U}_l(\xi,\eta,t)$ by $\widehat{c}_{l,ki}$ for $k=0,\ldots,p$ and $i=0,\ldots,k$ and for $l=1,2$. Mapping the numerical solution on each triangular cell to the (ζ,σ) coordinate system using (16) we find that we can write the semi discrete DG formulation (18) as the following system for the solution coefficients $\widehat{c}_{l,ki}$

$$\frac{d}{dt}\widehat{c}_{1,ki} = \frac{||\mathbf{a}||}{h}\left(\iint_{\Omega_0}\widehat{U}_1\left[\theta\frac{\partial}{\partial\xi}\psi_{ki}+(1-\theta)\frac{\partial}{\partial\eta}\psi_{ki}\right]\,dA-\int_0^1\widehat{U}_1(1-s,s,t)\psi_{ki}(1-s,s)\,ds\right.$$
$$\left.+(1-\theta)\int_0^1\widehat{U}_2(1-s,0,t)e^{-\Delta y\kappa_y}\psi_{ki}(s,0)\,ds+\theta\int_0^1\widehat{U}_2(0,s,t)e^{-\Delta x\kappa_x}\psi_{ki}(0,1-s)\,ds\right), \quad (22)$$

$$\frac{d}{dt}\widehat{c}_{2,ki} = -\frac{||\mathbf{a}||}{h}\left(\iint_{\Omega_0}\widehat{U}_2\left[\theta\frac{\partial}{\partial\xi}\psi_{ki}+(1-\theta)\frac{\partial}{\partial\eta}\psi_{ki}\right]\,dA-\int_0^1\widehat{U}_1(s,1-s,t)\psi_{ki}(1-s,s)\,ds\right.$$
$$\left.+(1-\theta)\int_0^1\widehat{U}_2(s,0,t)\psi_{ki}(s,0)\,ds+\theta\int_0^1\widehat{U}_2(0,1-s,t)\psi_{ki}(0,1-s)\,ds\right), \quad (23)$$

where $h=\frac{||\mathbf{a}||\Delta x\Delta y}{a\Delta y+b\Delta x}$ and $\theta=\frac{a\Delta y}{a\Delta y+b\Delta x}$. We can write this system in the following vector notation

$$\begin{aligned}\frac{d}{dt}\mathbf{c} &= \frac{||\mathbf{a}||}{h}\left[A+e^{-\Delta x\kappa_x}B+e^{-\Delta y\kappa_y}C\right]\mathbf{c},\\ &= \frac{||\mathbf{a}||}{h}\widehat{L}\mathbf{c},\end{aligned} \quad (24)$$

where $\mathbf{c}=[c_{1,00},\ldots,c_{1,pp},c_{2,00},\ldots,c_{2,pp}]^T$, A, B, and C are $(p+1)(p+2)\times(p+1)(p+2)$ matrices depending on the parameter θ, and $\widehat{L}=A+e^{-\Delta x\kappa_x}B+e^{-\Delta y\kappa_y}C$. Using the semi-discrete system (24), we can compute the complete spectrum of the DG spatial operator by computing the eigenvalues of $\widehat{L}$ over all possible choices of $\exp(\Delta x\kappa_x)$ and $\exp(\Delta y\kappa_y)$ being N-th and M-th roots of unity, respectively. That is, recalling that $\Delta x=\frac{1}{N}$ and $\Delta y=\frac{1}{M}$, we set $\kappa_x=2\pi ni$ and $\kappa_y=2\pi mi$ for $n=1,\ldots N$ and $m=1,\ldots,M$ and compute the $(p+1)(p+2)$ eigenvalues of $\widehat{L}$, which we label $\lambda_{knm}(\theta)$ for $k=1,\ldots,(p+1)(p+2)$. The complete spectrum of the DG spatial operator is then the collection of all $NM(p+1)(p+2)$ values $\lambda_{knm}(\theta)$. In Figures 5 and 6 we plot the spectral values $\lambda_{knm}(\theta)$ of the DG spatial operator for $p=1$ and $p=2$, respectively, with $N=M=10$, and for several values of θ. We note that, unsurprisingly, the shape of the spectrum is symmetric with respect to θ around $\theta=\frac{1}{2}$.

The spectral values in Figures 5 and 6 reveal that the overall size of the spectrum of the DG spatial operator is not particularly sensitive to the parameter θ. To observe this more directly, we compute the maximum magnitude of the spectral values

$$\lambda_{\max}(\theta)=\max_{k,n,m}|\lambda_{knm}(\theta)|,$$

as a function of θ. We then scale this function by the maximum value obtained by $\lambda_{\max}$ over $\theta\in[0,1]$ and plot this scaled function for $p=0,\ldots,5$ in Figure 7. In this figure, we see the largest maximum magnitude of the spectral values $\lambda_{\max}(\theta)$ is attained when $\theta=0,1$, and for every other values of θ the maximum magnitude of the spectral values is within 6% of this extremum.

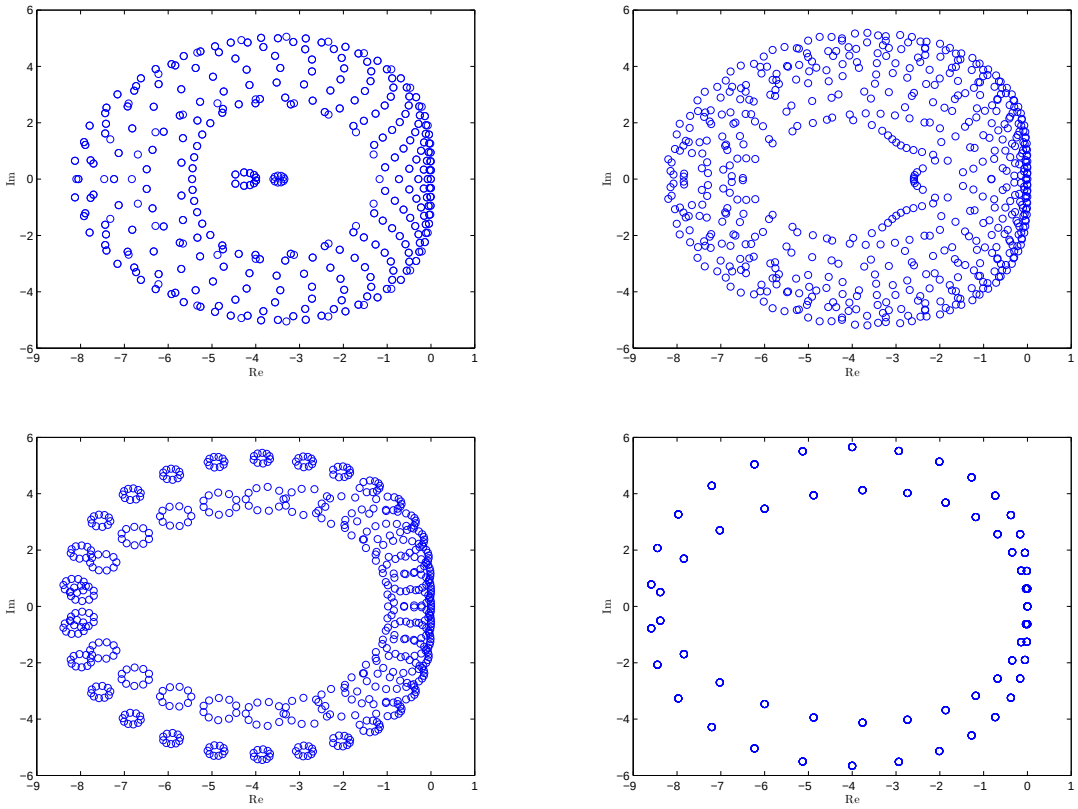

Figure 5: Spectral values $\lambda_{knm}(\theta)$ of the 2D spatial DG discretization for the linear advection equation, for the $p = 1$ with $N = M = 10$. We show the spectral values with $\theta = 0.5$ and 0.65 (top) and $\theta = 0.85$ and 1 (bottom).

We therefore observe that the spectrum of the DG spatial operator is directly scaled by the length h, while not being particularly sensitive to the relative direction parameter θ. These observation motivate us to propose a new CFL condition for the DG scheme applied to the linear advection problem in two dimensions on triangular meshes

$$\Delta t \leqslant CFL \min_j \frac{h_j}{||\mathbf{a}||}, \tag{25}$$

where the minimum stable time step Δt is now scaled by this new parameter h_j, which is the width of the cell Ω_j along the direction of flow. In the next section, we will investigate appropriate CFL numbers for this new CFL condition.

5 CFL Numbers

5.1 Explicit Runge-Kutta Time Integration

When we pair the semi-discrete DG scheme (15), on the uniform mesh of triangles described above, with an explicit order ν Runge-Kutta time integration scheme we will have that the method will

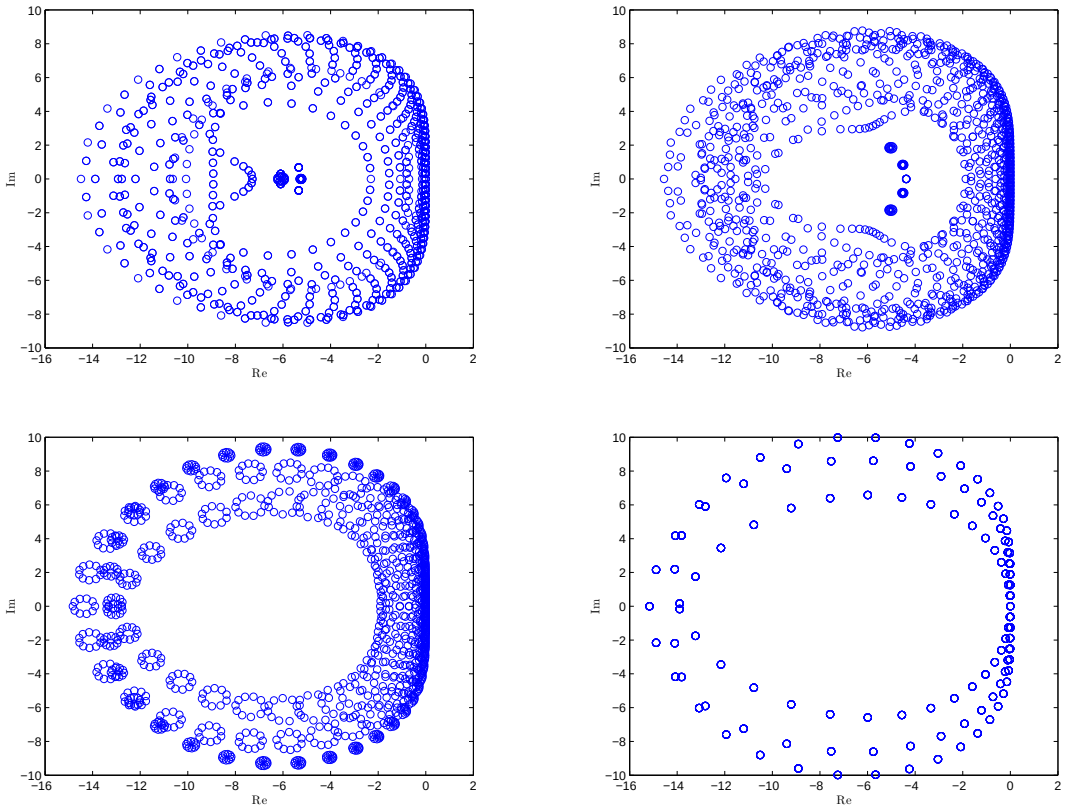

Figure 6: Spectral values $\lambda_{knm}(\theta)$ of the 2D spatial DG discretization for the linear advection equation, for the $p = 2$ with $N = M = 10$. We show the spectral values with $\theta = 0.5$ and 0.65 (top) and $\theta = 0.85$ and 1 (bottom).

be stable if Δt can be chosen sufficiently small so that

$$\frac{||\mathbf{a}||\Delta t\lambda_{knm}}{h} \in \mathcal{A}_\nu,$$

for all spectral values λ_{knm}, where $\mathcal{A}_\nu$ is the absolute stability region of the explicit Runge-Kutta scheme of order ν. Using the CFL condition (25), we can write this condition as

$$CFL\lambda_{knm} \in \mathcal{A}_\nu, \tag{26}$$

for all spectral values λ_{knm}, and the scheme will be stable if we can find such a CFL number. The absolute stability region of a ν-stage order ν Runge-Kutta scheme[1] is defined by $\mathcal{A}_\nu = \{z \big| |R_\nu(z)| \leqslant 1\}$ where

$$R_\nu(z) = \sum_{l=0}^{\nu} \frac{z^l}{l!}. \tag{27}$$

[1]Explicit Runge-Kutta scheme where the number of stages s is equal to the order ν of the scheme do not exist for $\nu \geqslant 5$ [8] and the stability regions of these scheem becomes more complex than given in (27). However it is usual to use this simple stability region for this type of analysis (see [5]).

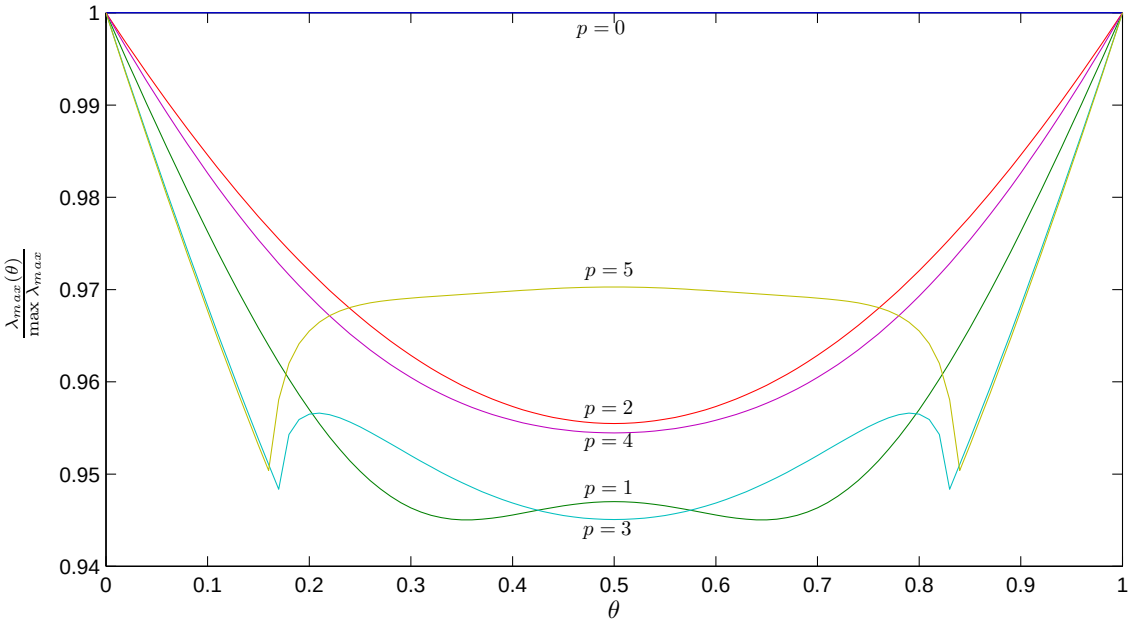

Figure 7: Ratio of the maximum in magnitude eigenvalue in the direction θ to the maximum in magnitude eigenvalue in the direction $\theta = 0$.

Therefore (26) will be satisfied when $|R_\nu(CFL\lambda_{knm})| \leqslant 1$ for all spectral values λ_{knm}. The spectral values λ_{knm} of course still depend on the parameter θ which give a measure of the direction of flow in each cell. However, as discussed above, the size of the spectrum is largest when $\theta = 0$ or 1. Hence we anticipate that finding a CFL number which yields a stable scheme when $\theta = 0$ should be within 5-6% of the true CFL number for other values of θ.

In Table 1 we compute the CFL number for the DG scheme of degree $p = 0, \ldots, 10$, with $\theta = 0$, paired with an explicit Runge-Kutta scheme of order $\nu = 1, \ldots 11$. The CFL numbers along the main diagonal of this table are of particular interest since in these cases the order of the spatial and temporal discretizations are the same. For one-dimensional schemes, it is in this case that we have the simple function $CFL = \frac{1}{2p+1}$ which gives a fairly tight bound on the true CFL numbers for $p = 0, \ldots, 10$. In this two dimensional case, our numerical tests have revealed that taking a CFL number given by

$$CFL = \frac{1}{(2p+1)\left(1 + \frac{4}{(p+2)^2}\right)}, \tag{28}$$

provides a fairly tight bound on the CFL number in the case when $\nu = p + 1$. We arrived at this expression in the following way. First, it appears that the size of the spectrum in two dimensions grows with respect to p at a similar rate to the one-dimensional spectrum, which requires the CFL number of $\frac{1}{2p+1}$. We therefore include this term in the two-dimensional CFL number. Several different function were then investigated to determine the remaining dependence on of the CFL number on p, including exponential, logarithmic, and certain rational functions. Ultimately the function $1 + \frac{4}{(p+2)^2}$ seemed to provide a tight bound, as well as having a fairly simple form. In Figure 8 we show this theoretical bound as a function of p together with the computed CFL numbers from

p	0	1	2	3	4	5	6	7	8	9	10
$\nu = 1$	0.500	-	-	-	-	-	-	-	-	-	-
$\nu = 2$	0.500	0.233	-	-	-	-	-	-	-	-	-
$\nu = 3$	0.628	0.278	0.165	0.109	0.079	0.059	0.047	0.038	0.031	0.026	0.023
$\nu = 4$	0.696	0.324	0.184	0.124	0.087	0.067	0.052	0.043	0.035	0.030	0.025
$\nu = 5$	0.804	0.365	0.212	0.141	0.101	0.077	0.060	0.047	0.038	0.031	0.027
$\nu = 6$	0.888	0.411	0.234	0.158	0.112	0.085	0.066	0.054	0.044	0.038	0.032
$\nu = 7$	0.989	0.452	0.261	0.174	0.124	0.095	0.074	0.060	0.049	0.042	0.036
$\nu = 8$	1.078	0.497	0.284	0.192	0.136	0.104	0.081	0.066	0.054	0.046	0.039
$\nu = 9$	1.175	0.539	0.310	0.208	0.148	0.113	0.088	0.072	0.059	0.050	0.042
$\nu = 10$	1.267	0.583	0.334	0.225	0.159	0.122	0.095	0.077	0.063	0.054	0.046
$\nu = 11$	1.363	0.626	0.359	0.241	0.171	0.131	0.102	0.083	0.068	0.058	0.049

Table 1: CFL numbers for DG methods of degree p paired with Runge-Kutta methods of order ν.

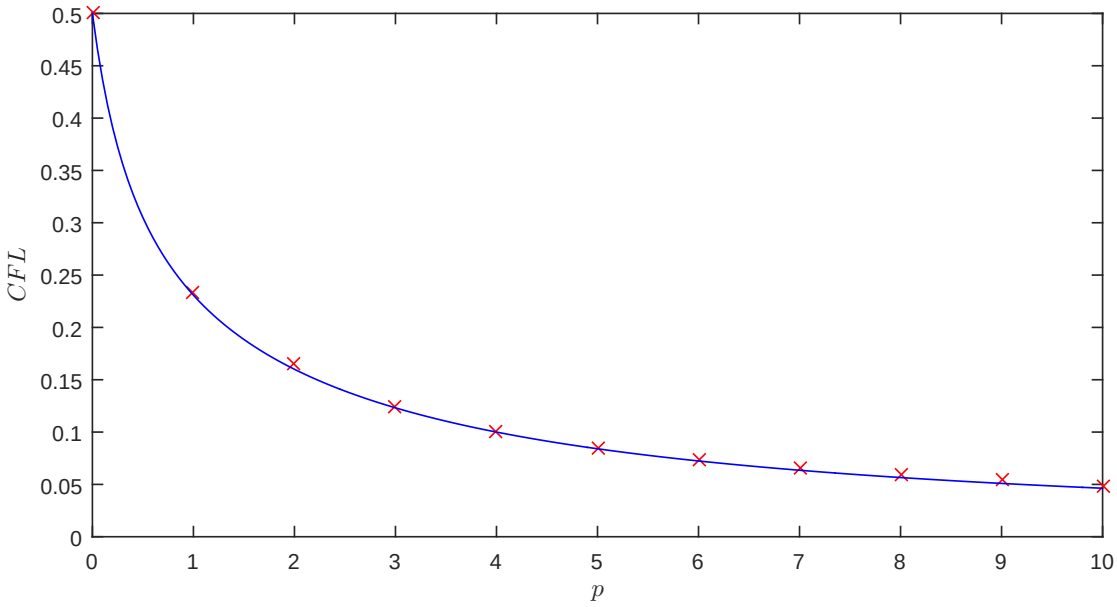

Figure 8: Plot of computed CFL numbers vs theoretical bound. We show the CFL values along the diagonal of Table 1 with the 'x' marker and the theoretical bound (28) as the solid line.

Table 1 when $\nu = p + 1$. We see from this figure that the bound (28) remains slightly below the computed CFL numbers in Table 1.

We note that the CFL condition usually implemented for the DG scheme on triangular meshes would bound Δt roughly as $\frac{1}{2p+1}\frac{r_j}{||\mathbf{a}||}$ where r_j is the radius of the inscribed circle in Ω_j or the length of the smallest edge in Ω_j, (25)-(28) would seem to be a significant improvement over the usual CFL condition. We see geometrically that r_j is a least half the size of h_j while $1 + \frac{4}{(p+2)^2} \leqslant 2$. In particular, we note that on our uniform mesh if the flow is parallel to an axis, say $b = 0$, we find that $\frac{h}{||\mathbf{a}||} = \frac{\Delta x}{a}$ and the time step restriction (25) will have no dependence on Δy. This implies that we are able to use a very fine mesh in the y direction without sacrificing the size of the time step

p	0	1	2	3	4	5	6	7	8	9	10
C_p	0.500	0.677	0.748	0.772	0.780	0.783	0.782	0.780	0.778	0.776	0.773

Table 2: Scaling factors C_p relating one- and two-dimensional spectra.

Δt, a fact we will demonstrate in the numerical examples section below.

5.2 Scaling within One-dimensional Spectrum

Since considerably more work has been done to investigate the spectrum of the one-dimensional DG scheme and to select efficient Runge-Kutta time integration schemes, we proceed in this section by finding a scaling of the two-dimensional DG spectrum so that it rests entirely within the spectrum of the one-dimensional DG discretization. With such a scaling, the results from works such as [12, 13] and [16] are immediately applicable to the two-dimensional scheme.

At first glace, the question of how to scale the two-dimensional spectrum to rest within the one-dimensional spectrum is a difficult one. Both spectra are a series of discrete points in the left-half of the complex plane and it is unclear precisely how to determine when one spectrum is 'inside' another. We answer this question by making use of a result from [10] which states that on a uniform mesh every spectral value λ of the one-dimensional spectrum satisfies

$$|F_p(\lambda)| = 1,$$

where $F_p(\lambda)$ is the $\frac{p}{p+1}$ Padé approximant [1] of the exponential function $e^{-\lambda}$. This expression partitions the complex plane into two regions. Complex numbers z inside the one-dimensional spectrum will satisfy $|F_p(z)| > 1$ and complex numbers outside the one-dimensional spectrum will satisfy $|F_p(z)| < 1$. We can therefore determine the scaling of the spectrum of the two-dimensional DG discretization by finding a number C_p such that

$$|F_p(C_p\lambda_{knm})| \geqslant 1,$$

for all spectral values λ_{knm} of the two-dimensional DG disctretization. We numerically determine these numbers C_p in the case when $\theta = 0$ and list them in Table 2 for $p = 0, \ldots, 10$. Using this scaling, we can apply any RK time integration scheme usually used in one dimension to the two-dimensional DG scheme, and such a time-stepping will be stable when

$$\Delta t \leqslant CFL_{1D} C_p \frac{h}{||\mathbf{a}||},$$

where CFL_{1D} is the usual CFL number used for the one-dimensional order $p+1$ DG scheme paired with the chosen RK method.

6 Extension to Non-linear Hyperbolic Systems

We conclude our analysis with some comments on how this proposed CFL condition can be extended to general non-linear hyperbolic systems. We consider the general two-dimensional hyperbolic system

$$\mathbf{u}_t + \nabla \cdot \mathbf{F}(\mathbf{u}) = 0 \tag{29}$$

subject to appropriate initial and boundary conditions in a region $\Omega \subset \mathbb{R}^2$. Here $\mathbf{F} = (\mathbf{F}_1, \mathbf{F}_2)$ is a tensor of two vector valued flux functions $\mathbf{F}_1(\mathbf{u})$ and $\mathbf{F}_2(\mathbf{u})$. Note that the system is assumed to be hyperbolic, that is, the matrix $\alpha A(\mathbf{u}) + \beta B(\mathbf{u})$ is diagonalizable and has real eigenvalues for any α and β such that $\alpha^2 + \beta^2 = 1$, where $A(\mathbf{u}) = (\mathbf{F}_1)_{\mathbf{u}}$ and $B(\mathbf{u}) = (\mathbf{F}_2)_{\mathbf{u}}$. As is usually done when considering the CFL condition for non-linear problems, we linearize the flux tensor $\mathbf{F}(\mathbf{U}_j)$ around the cell averages $\bar{\mathbf{U}}_j$ in Ω_j. We assume that the higher-order terms in this linearization are sufficiently small to be negligible so that we can consider the stability of the linear system

$$\frac{\partial \mathbf{U}_j}{\partial t} + A\frac{\partial \mathbf{U}_j}{\partial x} + B\frac{\partial \mathbf{U}_j}{\partial y} = 0,$$

on Ω_j where $A = \frac{d\mathbf{F}_1}{d\mathbf{u}}(\bar{\mathbf{U}}_j)$ and $B = \frac{d\mathbf{F}_2}{d\mathbf{u}}(\bar{\mathbf{U}}_j)$. Now in the particular case when the matrices A and B commute we will have that they are also simultaneously diagonalizable. Hence, through a change of variables $\mathbf{W}_j = R\mathbf{U}_j$, where the columns of R are the simultaneous eigenvectors of A and B, we can decouple the system into M equations where M is size of the system (29), i.e.

$$\frac{\partial \mathbf{W}_j}{\partial t} + D_1\frac{\partial \mathbf{W}_j}{\partial x} + D_2\frac{\partial \mathbf{W}_j}{\partial y} = 0,$$

where D_1 and D_2 are diagonal matrices. Denoting the vector $\mathbf{W}_j$ as $\mathbf{W}_j = [W_{1,j}, W_{2,j}, \ldots, W_{M,j}]^T$, and the diagonal elements of D_1 and D_2 as a_k and b_k, respectively, for $k = 1, \ldots, M$, we can write this system as M characteristic equations

$$\frac{\partial W_{k,j}}{\partial t} + a_k\frac{\partial W_{k,j}}{\partial x} + b_k\frac{\partial W_{k,j}}{\partial y} = 0,$$

for $k = 1, \ldots, M$. We can then consider the CFL condition associated with each of these independent equations. That is, we calculate the parameter $h_{k,j}$ associated with the k-th characteristic field's velocity $\mathbf{a}_k = [a_k, b_k]^T$, and take the time step Δt to be bounded by the smallest of all the $h_{k,j}$,

$$\Delta t \leqslant CFL \min_{j,k} \frac{h_{k,j}}{||\mathbf{a}_k||}. \tag{30}$$

In the more general case when the matrices A and B do not commute, some characteristic fields will not have a unique flow direction. Rather, these fields will have an infinite set of flow directions forming a characteristic Monge cone. For these fields, we can extend our proposed CFL condition by considering all directions and minimizing the cell width divided by the flow velocity of each field over all directions. An alternative option is simply to take $h_{k,j}$ to be the minimum height of the cell Ω_j, $h_{\min,j}$, and $||\mathbf{a}_k||$ to be the largest flow velocity of the field over all possible directions. Using either of these approaches in the calculation of h_j in (30) should be sufficient to obtain a linearly stable time step.

7 Numerical Examples

Our numerical tests aim to compare the CFL condition proposed above, which is scaled by the parameter h_j, to the usual CFL condition which is scaled by the radius of the inscribed circle in the cell. We will present both linear and non-linear examples for several degrees p and on both uniform

and non-uniform meshes to demonstrate its efficacy. In each example, we pair the order $p+1$ DG discretization with an explicit RK-$(p+1)$ time integration scheme and do not apply a limiter. We apply the method to each problem twice, once with the usual CFL condition and again with our proposed condition noting that both choices are indeed stable, and compare the number of time steps required to reach the final time T.

Linear advection, unstructured mesh

For the first linear test we consider the problem

$$u_t + u_x + u_y = 0, \tag{31}$$

on the square $\Omega = \{0 \leqslant x \leqslant 1, 0 \leqslant y \leqslant 1\}$ with periodic boundary conditions and with the initial condition consisting of a square pulse,

$$u(x, y, 0) = \begin{cases} 1, & 0.1 \leqslant x \leqslant 0.3, \;\; 0.1 \leqslant y \leqslant 0.3 \\ 0, & \text{otherwise.} \end{cases} \tag{32}$$

We apply the DG method on an unstructured mesh of 26524 elements up to a final time of $T = 0.5$ for several orders p. Using the usual time step restriction (2) which uses the radius of the inscribed circle in Ω_j we find that the $p = 1, 2$, and 3 schemes required 1187, 1978, and 2768 time steps, respectively, to reach the final time. In comparison, using our proposed CFL condition (25) we find that the $p = 1, 2$, and 3 schemes required 715, 1032, and 1340 time steps, respectively, to reach the final time. Since the computational cost of the scheme is directly proportional to the number of time steps required, this marks a significant increase in the efficiency of the algorithm. Indeed, at $p = 3$ the proposed time step reduces the amount of time steps required by more than 50%.

Linear advection, aligned structured mesh

It was remarked above that since h_j is geometrically the width of the cell Ω_j along the direction of flow $\mathbf{a}$ then h_j has no dependence on the size of Ω_j in an orthogonal direction. This implies that the mesh can be refined indefinitely in this dimension without further restricting the time step of the method. To observe this we consider a particularly simple example. We consider the linear advection problem

$$u_t + u_x = 0, \tag{33}$$

on the unit square with periodic boundary conditions and the square pulse initial condition (32). We apply the DG method on the uniform mesh described above with $\Delta x = \frac{1}{50}$ and $\Delta y = 1250$ for a total of 25000 cells. The mesh is therefore five times more refined in the y direction and classically we would expect this level of refinement to be the limiting factor in the time step restriction. Computing h_j, however, reveals that it has no dependence on Δy. Therefore when using the time step restriction (2) involving the radius of the inscribed circle we find that the $p = 1, 2$, and 3 schemes required 833, 1388, and 1943 time steps, respectively, to reach the final time of $T = 0.5$ while the scheme using our proposed time step (25) requires only 109, 157, and 204 time steps, respectively. We see that our proposed CFL condition achieves more than an 85% reduction in computational cost in this special case. This case demonstrates that h_j is an appropriate scaling in the CFL condition of the two-dimensional DG scheme since this stable time step would not have been predicted using previously proposed measures of cell size.

Burgers' equation, unstructured mesh

We proceed with two non-linear examples. For the first, we consider Burgers' equation in two dimensions,

$$u_t + uu_x + uu_y = 0, \tag{34}$$

on the unit square with periodic boundary conditions and with the initial condition consisting of a centered Gaussian pulse,

$$u(x, y, 0) = \exp\left(-15((x - 0.5)^2 + (y - 0.5)^2)\right). \tag{35}$$

We apply the DG method on an unstructured mesh of 41416 elements up to a final time of $T = 0.1$, before the formation of a shock. Using the usual time step restriction (2) involving the radius of the inscribed circle in Ω_j we find that the $p = 1, 2$, and 3 schemes required 265, 442, and 619 time steps, respectively, to reach the final time. In comparison, using our proposed CFL condition (25) we find that the schemes required 148, 213, and 276 time steps, respectively.

Euler equations, unstructured mesh

Finally, in our second non-linear example we consider the Euler equations in two dimensions,

$$\frac{\partial}{\partial t}\begin{pmatrix}\rho\\ \rho u\\ \rho v\\ E\end{pmatrix} + \frac{\partial}{\partial x}\begin{pmatrix}\rho u\\ \rho u^2 + P\\ \rho uv\\ u(E + P)\end{pmatrix} + \frac{\partial}{\partial y}\begin{pmatrix}\rho v\\ \rho uv\\ \rho v^2 + P\\ v(E + P)\end{pmatrix} = 0, \tag{36}$$

on the square $\Omega = \{-10 \leqslant x \leqslant 10, -10 \leqslant y \leqslant 10\}$ with the equation of state

$$P = (\gamma - 1)\left(E - \frac{1}{2}\rho(u^2 + v^2)\right), \tag{37}$$

and the initial condition consisting of a smooth vortex centered at the origin and moving upward, i.e.

$$\rho_0 = \left[1 - \frac{S^2M^2}{8\pi^2}\exp\left(\frac{1 - x^2 - y^2}{R^2}\right)\right]^{\frac{1}{\gamma-1}}, \tag{38}$$

$$u_0 = \frac{Sy}{2\pi R}\exp\left(\frac{1 - x^2 - y^2}{2R^2}\right), \tag{39}$$

$$v_0 = 1 - \frac{Sx}{2\pi R}\exp\left(\frac{1 - x^2 - y^2}{2R^2}\right), \tag{40}$$

$$P_0 = \frac{1}{\gamma M^2}\left[1 - \frac{S^2M^2}{8\pi^2}\exp\left(\frac{1 - x^2 - y^2}{R^2}\right)\right]^{\frac{\gamma}{\gamma-1}}, \tag{41}$$

where $S = 13.5$, $M = 0.4$, $R = 1.5$, and $\gamma = 1.4$. We use the constant boundary condition

$$\begin{pmatrix}\rho\\ u\\ v\\ P\end{pmatrix} = \begin{pmatrix}1\\ 0\\ 0\\ \frac{1}{\gamma M^2}\end{pmatrix} \tag{42}$$

along the boundary of the mesh.

We apply the DG method on an unstructured mesh of 16954 elements up to a final time of $T = 4$. Note that, as discussed above, since this system is not simultaneously diagonalizable there exist characteristics which do not degenerate to lines. We therefore take h_j to be the minimum height of the cell for these fields. Using the usual time step restriction (2) involving the radius of the inscribed circle in Ω_j we find that the $p = 1, 2$, and 3 schemes required 1387, 2312, and 3236 time steps, respectively, to reach the final time. In comparison, using our proposed CFL condition (25) we find that the schemes required 847, 1222, and 1587 time steps, respectively.

8 Discussion

In this paper, we have proposed a new CFL condition for the DG method applied to hyperbolic problems on triangular meshes. This condition is scaled by a parameter h_j, which geometrically is the width of the cell Ω_j in the direction of characteristic flow, rather than the usual inscribed radius in each cell. The justification for considering this CFL condition arises from (18) where the spatial operator of the DG scheme in each cell is scaled by the small parameter $\frac{1}{h_j}$. We apply classical von Neumann analysis on a uniform mesh of triangles and derive a simple linear system which can be used to calculate the spectrum of the entire DG spatial discretization. We compute the spectrum of the DG spatial operator and find that the size of the spectrum is scaled by h_j, and that while the spectrum depends on an additional parameter θ the overall size of the spectrum is not very sensitive to its value. We therefore propose a new CFL condition where the time step is scaled by h_j.

The proposed CFL condition (3) is local to each element and requires little additional computational effort to compute at each time step for linear and certain non-linear problems. For more general non-linear systems, an optimization can be performed to find the proper scaling for each characteristic field in each cell. This can be avoided, however, by using the smallest cell width which is potentially more restrictive than necessary. We propose the CFL number (28) in the case where the usual pairing of the order $p + 1$ DG discretization with an order $p + 1$ explicit Runge-Kutta scheme is implemented. This CFL number provides a functional relation with the order p which can be integrated into existing codes.

We use the proposed measure of cell size to compute a factor that scales the two-dimensional spectrum inside the spectrum of DG spatial operator in one dimension. With this scaling we can employ previous results concerning the linear stability of the one-dimensional scheme to the two-dimensional case and, in particular, use previously computed CFL numbers for several Runge-Kutta time discretizations specifically developed for DG schemes [12, 13, 16].

In our numerical examples we show that the proposed CFL condition provides linearly stable schemes on unstructured grids for both linear and non-linear problems. The CFL condition also provides larger time steps than the CFL condition which uses the radius of the inscribed circles, and the gains of which increase with the order of approximation. As a consequence of the measure h_j depending on the direction of flow, we also show an example where the mesh can be continuously refined along a certain dimension while not affecting the stability of the scheme. This can potentially be useful when considering mesh refinement strategies in problems with anisotropic meshes, e.g. a mesh stretched along a surface of an airfoil. This idea will be explored in a future work.

9 Acknowledgment

This research was supported in part by the Natural Sciences and Engineering Research Council (NSERC) of Canada grant 341373-07.

References

[1] G. A. Baker and P. R. Graves-Morris. *Padé Approximants*. Addison-Wesley, Reading, Mass.; Don Mills, Ont., 1981.

[2] N. Chalmers, L. Krivodonova, and R. Qin. Relaxing the CFL number of the discontinuous Galerkin method. *SIAM Journal on Scientific Computing*, 36(4):A2047–A2075, 2014.

[3] B. Cockburn, S. Hou, and C.-W. Shu. The Runge-Kutta local projection discontinuous Galerkin finite element method for the conservation laws IV: The multidimensional case. *Mathematics of Computation*, 54:545–581, 1990.

[4] B. Cockburn and C.-W. Shu. The Runge-Kutte local projection P^1 discontinuous Galerkin method for scalar conservation laws. *RAIRO Model. Math. Anal. Numer.*, 25:337–361, 1991.

[5] B. Cockburn and C.-W. Shu. Runge-Kutta discontinuous Galerkin methods for convection-dominated problems. *Journal of Scientific Computing*, 16:173–261, 2001.

[6] M. Dubiner. Spectral methods on triangles and other domains. *Journal of Scientific Computing*, 6(4):345–390, 1991.

[7] D.A. Dunavant. High degree efficient symmetrical Gaussian quadrature rules for the triangle. *International Journal for Numerical Methods in Engineering*, 21(6):1129–1148, 1985.

[8] E. Hairer, S.P. Norsett, and G. Wanner. *Solving Ordinary Differential Equations I. Nonstiff problems*. Springer, Berlin, second edition, 2000.

[9] J. S. Hesthaven and T. Warburton. *Nodal Discontinuous Galerkin Methods. Algorithms, Analysis, and Applications*. Springer, 2007.

[10] L. Krivodonova and R. Qin. An analysis of the spectrum of the discontinuous Galerkin method. *Applied Numerical Mathematics*, 64:1–18, 2013.

[11] E.J. Kubatko, C. Dawson, and J.J. Westerink. Time step restrictions for Runge–Kutta discontinuous Galerkin methods on triangular grids. *Journal of Computational Physics*, 227(23):9697–9710, 2008.

[12] E.J. Kubatko, J.J. Westerink, and C. Dawson. Semi discrete discontinuous Galerkin methods and stage-exceeding-order, strong-stability-preserving Runge–Kutta time discretizations. *Journal of Computational Physics*, 222(2):832–848, 2007.

[13] E.J. Kubatko, B.A. Yeager, and D.I. Ketcheson. Optimal strong-stability-preserving Runge–Kutta time discretizations for discontinuous Galerkin methods. *Journal of Scientific Computing*, 60(2):313–344, 2014.

[14] J. Niegemann, R. Diehl, and K. Busch. Efficient low-storage Runge–Kutta schemes with optimized stability regions. *Journal of Computational Physics*, 231(2):364 – 372, 2012.

[15] T. Toulorge and W. Desmet. CFL conditions for Runge–Kutta discontinuous Galerkin methods on triangular grids. *Journal of Computational Physics*, 230(12):4657–4678, 2011.

[16] T. Toulorge and W. Desmet. Optimal Runge-Kutta schemes for discontinuous Galerkin space discretizations applied to wave propagation problems. *Journal of Computational Physics*, 231(4):2067 – 2091, 2012.

[17] T. Warburton and T. Hagstrom. Taming the CFL number for discontinuous Galerkin methods on structured meshes. *SIAM Journal on Numerical Analysis*, 46(6):3151–3180, 2008.